Roger L. Verkuil Huntington W. Curtis Mun S. Pak

# A Contactless Method for High-Sensitivity Measurement of p-n Junction Leakage

A contactless p-n junction leakage measurement method is described that uses low-noise vhf oscillator circuitry to examine the dynamic memory-like behavior of the junctions. This method utilizes the eddy current loading effect, via inductive coupling, in order to determine the leakage-dependent decay time of the photoinduced voltage across the diffused p-n junctions. The contactless measurement is made under low forward bias conditions ( $\leq 10 \text{ mV}$ ) such that this measurement is a function of only generation-recombination processes in the junction depletion region. In the low-noise circuitry, sensitivity is enhanced when the oscillatory amplitude is made directly proportional to the figure of merit Q of the coupled oscillator resonant LC tank. This simple oscillator circuit contains only one JFET and a small number of inductors and capacitors, and is supplied by a constant-current source. Junction decay times between  $10^{-4}$  and 1 s, corresponding to junction leakages between  $10^{-6}$  and  $10^{-10}$ A/cm<sup>2</sup>, respectively, have been measured and are in excellent agreement with the derived theory showing the contactless decay time to be inversely proportional to the conventional contacting reverse leakage.

#### Introduction

Dynamic memory storage devices such as single-cell p-n junctions use the principle of charge storage, which is achieved by momentarily impressing a high- or low-voltage state across each junction. This charge is maintained by periodically sensing the state and restoring ("refreshing") any small portion of charges that are gradually lost due to various leakage mechanisms. Some examples of leakage mechanisms are crystal defects, metallic impurities, and inversion layers that are severe enough for the charge state to be lost before being refreshed. While this problem of the loss of charge state can be minimized by arbitrarily increasing the refresh rate at the expense of having less time available for actual memory use, it is far more desirable to minimize the leakage mechanisms, which typically originate during semiconductor wafer processing. Any efforts to reduce and control these process-induced leakages will, however, require some convenient in-process means of monitoring the leakage in question. Conventional probing methods for determining leakage pose monitoring problems in terms of 1) lengthy measurement time required for probing a representative number of junctions, 2) undesirable contamination and damage from the probes, 3) inability to contact junctions normally covered by dielectric layers during most of the process, and 4) inability to measure extremely low-level leakages that are easily rendered in error by background leakage associated with the probing apparatus. In contrast, the above leakage-measurement problems can be easily avoided with the noncontacting measurement described in this paper, which features the dynamic memory behavior of p-n junctions.

A very-high-frequency (vhf) oscillator, inductively coupled to the wafer, is used to examine the median relaxation time of small photoinduced voltages across a plurality of junctions in a noncontacting mode by means of the eddy current loading effect. As will be shown, the small photovoltage is a necessary restriction that in turn requires extremely sensitive, high signal-to-noise (S/N) circuitry, which exploits the so-called marginal oscillator concept [1]. The goals of this paper are to demonstrate theoretically and empirically that relatively voltage-inde-

Copyright 1980 by International Business Machines Corporation. Copying is permitted without payment of royalty provided that (1) each reproduction is done without alteration and (2) the *Journal* reference and IBM copyright notice are included on the first page. The title and abstract may be used without further permission in computer-based and other information-service systems. Permission to *republish* other excerpts should be obtained from the Editor.

pendent leakage currents can be rapidly and conveniently monitored by a noncontacting technique, and to present the novel instrumentation required to practice this technique.

This technique has been practiced for several years as an early in-line monitor in semiconductor bipolar logic and static memory programs at IBM. It has been successful as a means of detecting leakage problems such as those associated with metallic contamination in epitaxial silicon and reactive ion etching processes, with incomplete collector-to-collector isolation, with defects from oxygen precipitation in the bulk of the silicon wafer, and with contaminants from wet chemicals commonly used in semiconductor processing. However, the technique has not as yet been tried in a dynamic memory process line, although we feel that examining dynamic memory product wafers with a technique based on dynamic memory is fitting, and that it may prove to be as useful in this application as it has been in other technologies.

## **Experimental procedures**

#### • Contacting measurements

The reverse-leakage current of p-n junctions on each of a number of wafers was measured by the conventional *I-V* technique using a commercial picoammeter. Czochralskigrown Si wafers (11-25  $\Omega$ -cm, 82 mm in diameter, 0.4 mm thick) were fabricated with the configuration of p-n junctions shown in Fig. 1. In addition to the many small-area junctions on the wafers, several large test junctions ( $\approx$ 0.04 mm² in area) were used to provide leakage currents high enough to be easily measured by the picoammeter. Metallized platinum silicide contacts were used to avoid point-contact diode effects between the probe tips and the silicon. All junctions were formed with an n¹ arsenic diffusion. A p-type isolation diffusion (not shown) was used to avoid conductive surface channels between the n¹ diffusions.

The reverse-leakage currents of three large test junctions within the central 30-mm-diameter region of each wafer were measured using contacting probes and the picoammeter. The median leakage current obtained for each wafer was used to represent that wafer in later comparisons with noncontacting measurements.

The leakage current was measured at a reverse bias of 0.1 V. This relatively low voltage condition was a compromise in terms of being large enough to measure reverse saturation leakage and small enough to minimize field-enhanced leakage mechanisms. The reader is referred to the Theory and Discussion sections for more details.

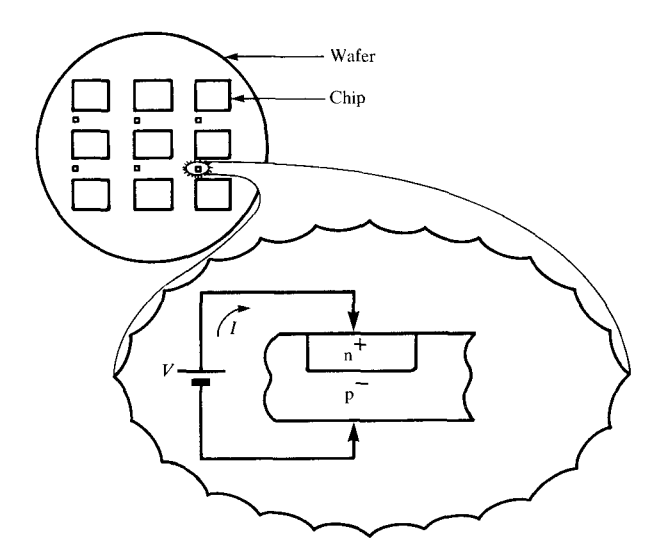


Figure 1 Configuration of the test junctions.

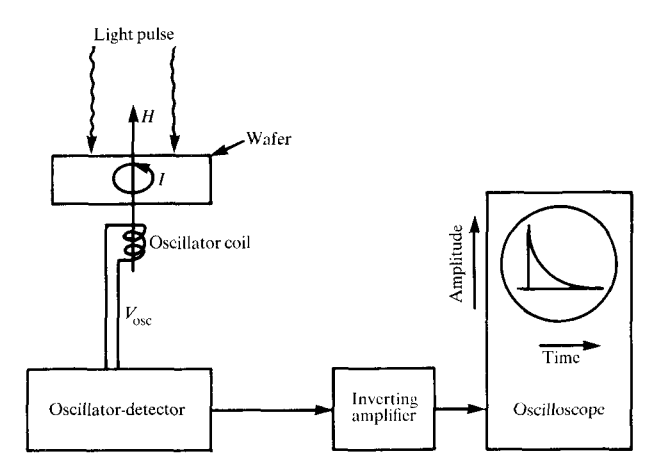


Figure 2 Block diagram of the tool used to measure contactless p-n junction decay times.

## • Noncontacting measurements

The contactless p-n junction decay time measurements were performed with the inductive coupling "eddy current technique" illustrated in Fig. 2. The figure shows a Si wafer in close proximity to the coil of a vhf oscillator whose LC tank Q-controlled amplitude is sensitive to the changes in impedance produced in the p-n junctions when they are perturbed by light (see Theory section). These small changes in amplitude are converted to instantaneous output level changes by means of self-detection in the oscillator circuit and are then ac coupled to a high-gain wideband inverting amplifier for subsequent display on an oscilloscope. This oscillator circuit, which has been opti-

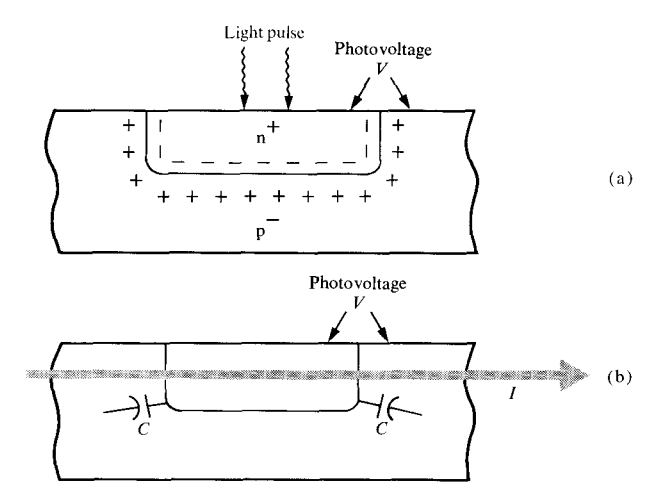


Figure 3 The effect of light-induced p-n junction voltage on eddy currents. (a) The solar cell effect; (b) the junction capacitance effect on oscillator loading, where I, the eddy current due to emfs (not shown) from vhf coupling, is modulated by C = f(V).

mized for high sensitivity to small impedance changes and for low noise, is presented in detail in Ref. [2] and is summarized in the Appendix of this paper.

No special sample preparation was required for the contactless decay time measurement. The wafers were in the same physical state as previously described for the contacting measurement of leakage current. The central 30-mm-diameter region of each wafer was measured. This area corresponds to the effective coupling area of the oscillator coil. The decay-time measurement was indicative of the ''median-like'' decay-time behavior of every junction within the measurement area.

Each wafer was tested on the contactless eddy current tool in order to measure the "p-n junction decay time." A light-emitting diode (LED) was used as the pulsed-illumination source. The red light ( $\lambda=0.63~\mu m$ ), with a maximum penetration depth of  $\approx 5~\mu m$ , was used to excite only the p-n junctions, not the bulk semiconductor material, and had a pulse duration of 5 ms and an "off time" in excess of 1 s. The intensity of the LED was gradually reduced to a level where the decay-time trace became exponential and the decay time constant  $\tau$  became independent of further reductions in intensity. This procedure ensured a peak photoinduced p-n junction potential of  $\leq 10~mV$  (see Theory section).

## Theory

### • Photovoltaic behavior of p-n junctions

When light impinges on a Si wafer that is populated with p-n junctions, the resultant electron-hole pairs generated in junction depletion regions contribute to the creation of a forward potential across the junctions, as in the common solar cell effect. The light-induced forward potential rises to an equilibrium value when the light is on and decays to zero when the light is off.

# • Eddy current loading effect

The ability to observe the photovoltaic behavior of p-n junctions in a noncontacting fashion is due to the eddy current loading effect that the p-n junctions impose on the vhf oscillator circuitry discussed previously. The timevarying magnetic field from the oscillator coil penetrates the Si wafer and sets up time-varying electromotive forces (emfs) according to Faraday's law. The induced emfs impart motion to free electrons and holes (eddy current effect), which constitutes a power drain on the oscillator. The sensitivity of the oscillator to such power drains, due to its LC tank Q-controlled design, causes the amplitude of the oscillations to be reduced in direct proportion to the eddy current losses in the wafer. These losses are a function of the induced emfs, the concentration and mobility of the free carriers, and eddy current impedance paths including the p-n junction capacitive reactance.

## • Impact of p-n junctions.

As shown in Fig. 3, the p-n junctions are part of the impedance path of the eddy currents. Therefore, variations in junction capacitance C, as a function of the width of the depletion region, cause variations in the power absorbed by the wafer and thereby modulate the amplitude of the oscillator. This depletion width is sensitive to small changes in the light-induced p-n junction forward voltage [3]. These variations in depletion width affect the power absorbed by the wafer because of the following mechanisms: 1) the electrical thickness and hence, the conductance, of a wafer increases slightly when the depletion regions are reduced by forward bias; and 2) eddy currents due both to induced emfs across the high-resistivity side of the junctions and to emfs across the n<sup>+</sup> diffusions flow through the capacitive reactance of the p-n junctions and result in an absorbed power increase when the junction capacitance is increased by forward bias. The dominant effect in our experiment was due to eddy currents from the substantial emfs across the n<sup>+</sup> diffusions. This increase in current provided a S/N advantage that would not have been possible had we chosen capacitive, rather than inductive, rf coupling from the oscillator to the wafer. The contributions from the other mechanisms suffered from a low forward bias constraint and from the relatively lower emfs across the high-resistivity side of the junctions.

## • Model of decay transient

Illumination is used to set an initial forward potential across the junctions; this potential then decays when the

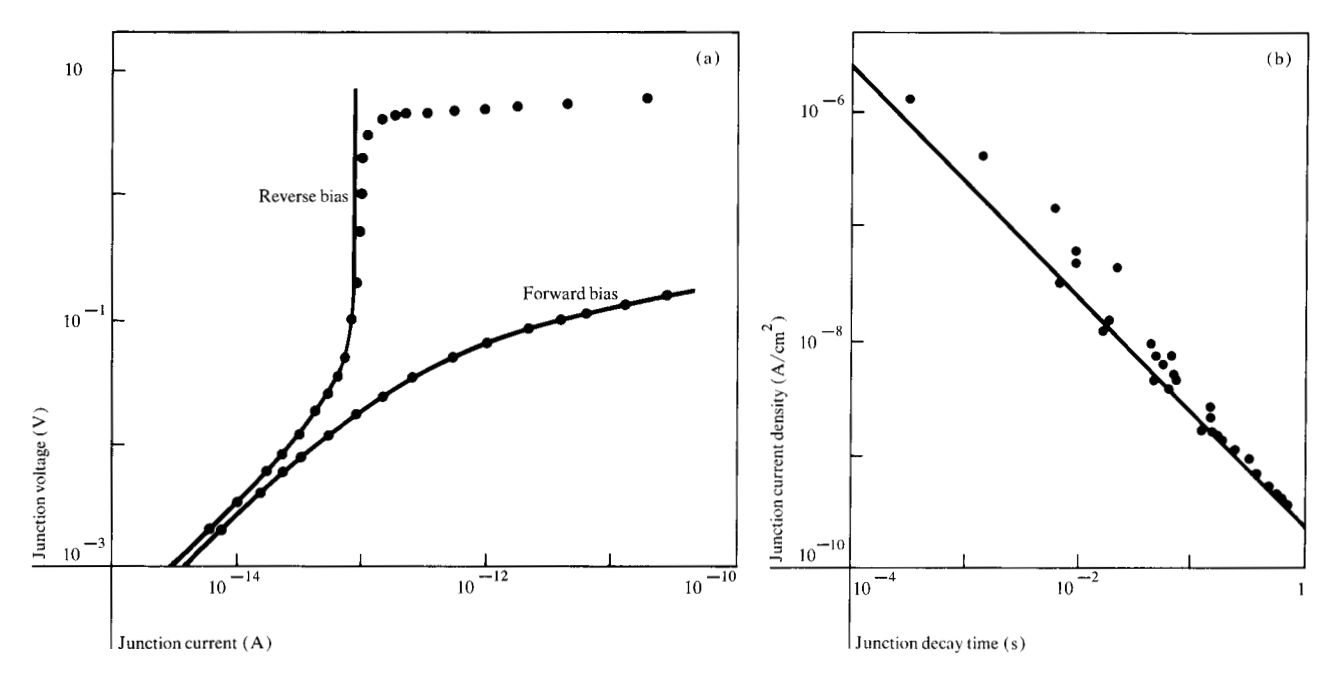


Figure 4 A comparison of the experimental (data points) and theoretical (—) (a) forward and reverse *I-V* characteristics of a typical p-n junction used in the study, and (b) relationship between the junction reverse current density (contacting measurement) and the p-n junction decay time (contactless measurement).

light is turned off. In our model this potential was considered to result from momentary contact to an external voltage source. An equivalent circuit of the p-n junction would contain a parallel combination of the initial forward voltage source  $V_0$ , the voltage-dependent capacitance C (F-cm<sup>-2</sup>), and the current density J of the junction, where J is assumed to obey the ideal diode law,

$$J = J_0 \left[ \exp\left( \frac{qV}{kT} \right) - 1 \right],\tag{1}$$

where  $J_0$  is the reverse saturation current (A/cm²), q is the electron charge (1.602 × 10<sup>-19</sup> C), k is Boltzmann's constant (8.62 × 10<sup>-5</sup> eV/K), and T is the absolute temperature (K). This assumption is borne out by the excellent fit between Eq. (1) and the experimental I-V characteristics; see Fig. 4(a). The same value of  $I_0$  (=  $J_0$  times the junction area A) was used to fit Eq. (1) to the forward and reverse data. The initial voltage across the junction  $V_0$  decays as a function of C and J.

The desired reverse leakage current to be measured in a noncontacting fashion is  $J_0$ . In order to determine  $J_0$ , it is necessary to establish a common physical basis between the contacting and noncontacting measurements. The total reverse (forward) current of a p-n junction in general can be approximated by the sum of diffusion components in the neutral regions and generation (recombination) components in the depletion region [4]. For Si at room temperature, the reverse current of a p-n junction is pri-

marily due to the depletion-region component [5]; however, for forward current this component is dominant only for very small bias conditions [6]. Therefore, in order to have this common physical basis (i.e., a strong dependence on depletion-region properties) for both types of measurement, a  $V_0 \le 10$  mV was chosen for the model.

The very small  $V_0$  required yields additional advantages. The voltage-dependent junction capacitance becomes virtually constant because the total change in C < 1% for the 10-mV excursion. Equation (1) also simplifies to  $J \approx J_0 q V/kT$  for  $V_0 \le 10$  mV < kT/q. Lastly, the model becomes independent of  $V_0$  (to be shown), which aids measurement reproducibility and simplifies the testing procedure.

By taking advantage of the above simplifications, we can now proceed with a basic circuit theory approach to develop an expression for the appropriate decay transient. By differentiating Gauss' law,

$$Q = CV, (2)$$

with respect to time t, we get

$$J = C \frac{dV}{dt} + V \frac{dC}{dt} \,. \tag{3}$$

By approximating for very low bias  $(V \le 10 \text{ mV})$  Eqs. (1) and (3) can be reduced to

373

$$J \approx CdV/dt. \tag{4}$$

Setting these equations equal to each other and solving for V, we get

$$V = V_0 \exp(-t/\tau), \tag{5}$$

where the time constant  $\tau$  (in s) is given by  $CkT/J_0q$ . Finally, by rearranging the expression for  $\tau$ , we get

$$J_0 = CkT/q\tau. (6)$$

Equation (6) is the model that describes the expected theoretical relationship between the contacting reverse junction leakage current  $J_0$  and the contactless measurement  $\tau$ , where  $\tau$  is defined as the p-n junction decay time. More specifically,  $\tau$  is the time for a decay-time trace, as viewed on an oscilloscope, to decay from its initial amplitude to approximately the 1/e point ( $\approx 37\%$ ). When such decay-time traces are plotted on a semilogarithmic scale, true exponential behavior is observed (straight lines) as predicted by the model.

#### • Results vs model

We now obtain the specific form of the model for our experiment by substituting the appropriate values of all constants in Eq. (6). For the junction capacitance C, an abrupt junction value is used because of the step-like nature of the  $\rm n^+$  arsenic diffusion. The value of C corresponding to a p-type wafer background concentration of  $10^{15}$  atoms/cm³ was used, yielding  $J_0 = 2.5 \times 10^{-10}/\tau$  A-cm $^{-2}$ .

The above model and the experimental data are plotted in Fig. 4(b); there is agreement between the model (solid line) and the experimental data points over a current range of approximately four decades.

#### Discussion

A number of considerations influenced this experiment. The possible influence of bulk detrapping effects on junction decay time was minimized by the shallow penetration depth of the red light used. A completely darkened environment was used to prevent stray light from interfering with the photovoltaic behavior from the low-intensity pulsed light source. A readily detectable signal was obtained by using high S/N circuitry in combination with increased junction eddy current from vhf inductive coupling. Additionally, erroneous surface leakage paths were eliminated with an isolation diffusion. Overloading of the LC tank Q-controlled oscillator was prevented by choosing small n<sup>+</sup> diffused regions (typical LSI situation), which minimized steady-state eddy current losses. A wide range of leakage values was obtained by using iron contamination and oxygen precipitation to create high and intermediate leakage values, respectively. Temperatures greater than room ambient were avoided in order to maintain the desired measurement sensitivity to the depletion region (generation-recombination regime) as opposed to the neutral region (diffusion regime). The sampling plan assumed a fair degree of leakage uniformity from junction to junction, which proved to be more valid for the lower-leakage wafers. Field-enhanced reverse leakage effects were minimized by using the low bias of 100 mV. For a higher (and more typical) bias of several volts, these effects, which could not be explained by the resultant increase in the depletion width of the junction, tended to make the contact-determined leakage of highleakage wafers exceed the predictions based on contactless measurements. We speculate that this behavior was due to field-enhanced defect leakage from Fe and O contamination enhanced by the high-perimeter field resulting from the close spacing of n<sup>+</sup>-p<sup>+</sup> diffusions in our samples. Preliminary studies in which this spacing was increased showed similar good agreement between theory and data at higher reverse bias.

There are a few other areas of investigation that might be pursued in a similar contactless fashion: e.g., examination of bulk phenomena by adjusting measurement conditions for operation in the diffusion regime, determination of resistive leakage, and reduction of coil or light-spot size to examine nonuniformities in leakage distribution.

We believe that our work demonstrates the ability for a noncontacting leakage measurement to be a good substitute, under appropriate conditions, for the more conventional contacting method. In addition, it is expected that this method could in some cases prove superior for ultralow-level measurement applications where contacting methods are hampered by stray leakage, and sampling problems associated with maverick leakage paths (a function of increasing junction area). The speed, ease, and extendability of the contactless measurement in general is compatible with the need for rapid, nondestructive diagnostic tools in an integrated-circuit process line.

#### **Conclusions**

Under low bias conditions, good agreement was obtained between contactless and contact methods of measuring p-n junction leakage currents. Both methods are keyed to the generation-recombination processes in the depletion region, which allows the theoretical treatment to be straightforward and shows excellent agreement with the experimental data.

## **Acknowledgments**

We are grateful to the late T. R. Lawson for his development of the simultaneous-solution program used to solve

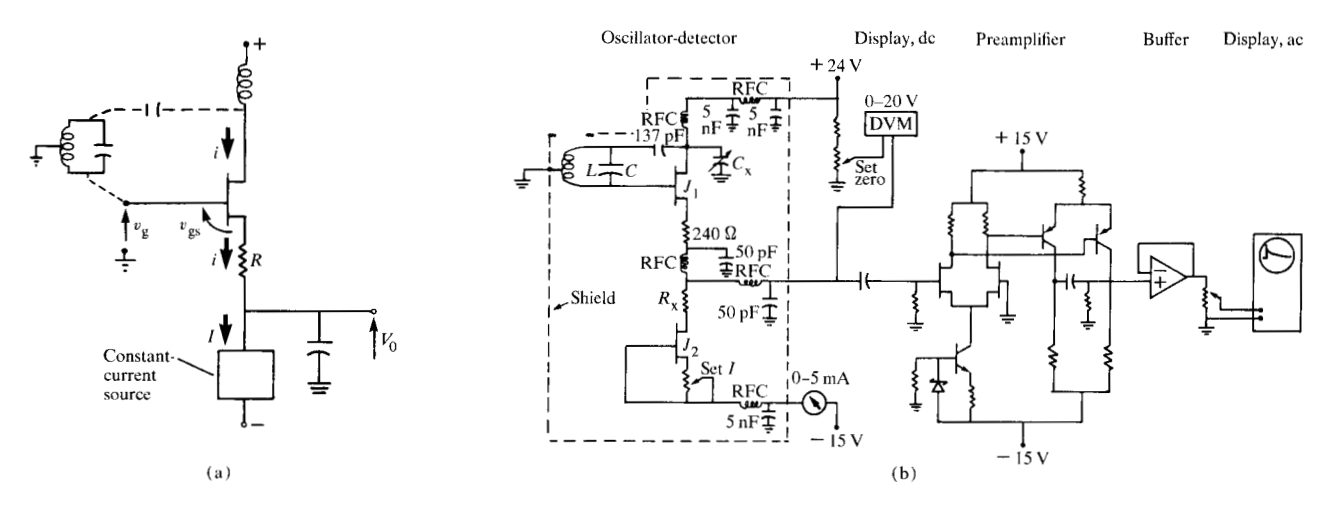


Figure A1 (a) Oscillator-detector supply current path, and (b) the practical circuit configuration.

our oscillator/detector transcendental modeling equations, and to S. Eros and G. F. Dolan for their encouragement and many hours of helpful discussions. There have been oral presentations of this work by the authors at the ASTM Symposium on Lifetime in Silicon, San Diego, CA, February 1979.

### Appendix: Oscillator detector circuit discussion

This appendix is a summary of the circuit principles and analysis of the apparatus on which the reported measurements were made. For these measurements, the time variation of voltage displayed on an output oscillograph is shown to be directly proportional to the time variation of photoinduced conductivity in a wafer electromagnetically coupled to a vhf oscillator coil. Since the photoinduced conductivity change is approximately four orders of magnitude smaller than the wafer conductivity, high sensitivity and low noise are design requirements; ability to follow conductivity changes from microseconds to many tenths of seconds requires broad-band design. The following sections address the dependence of oscillator tank Q on wafer conductivity, of oscillator tank voltage on Q, and of detector output voltage on tank voltage. By combining these relations one can predict the overall transfer function, the oscilloscope output as a measure of wafer conductivity.

## • Wafer conductivity and tank Q

When a semiconductor wafer is in proximity to an energized resonant LC tank circuit, the oscillating magnetic field of the inductor induces voltages that produce eddy currents within the semiconductor. The resulting power

loss in the semiconductor may be considered as power dissipated in a resistor added in series with the coil inductance. Quantitatively, if at resonant angular frequency  $\omega$  the uncoupled Q of the parallel LC tank is given by  $Q' = \omega L/R_{\rm s}$  ( $R_{\rm s}$  is the series ac resistance of the inductor and capacitor), then the value when coupled to a wafer becomes  $Q = \omega L/(R_{\rm s} + R_{\rm w})$ . Let  $R_{\rm w}$ , the reflected resistance due to the wafer, be equal to  $R_{\rm o} + r$ , where  $R_{\rm o}$  is due to the wafer in the dark and r is the additional resistance caused by photoconductivity effects and their variation (decay) with time. Letting  $Q_{\rm o} = \omega L/(R_{\rm s} + R_{\rm o})$ ,  $Q = Q_{\rm o}[1 - (r/R) + {\rm higher-order\ terms}]$ . Since r << R, one observes that photoinduced lowering of Q is directly proportional to the photoinduced increase in wafer conductivity; i.e.,

$$\Delta Q \approx k_1 r.$$
 (A1)

# Oscillator gate voltage amplitude

The basic oscillator-detector circuit [shown in Fig. A1(a)] is designed such that at resonance,  $\omega L >> R$  and its tank circuit has impedance  $Z = Q(L/C)^{1/2}$  at  $\omega = 1/[2\pi(LC)^{1/2}]$ . With the ground tap at the electrical center of inductor L, the impedance driven by the transistor drain is  $Z = [Q(L/C)^{1/2}]/4$ . If the drain approximates a constant ac current generator  $i_1 = I_1 \sin \omega t$ , the gate voltage will be  $v_g = V_g \sin \omega t$ , where  $v_g = [QI_1(L/C)^{1/2}]/4$ . For an idealized depletion-mode JFET transistor with threshold voltage  $V_T$  and transconductance  $g_m$ , the drain current will be a train of cosine pulses of conduction angle  $\phi$ . Only the Fourier fundamental component (identified by subscript 1), which is at the tank resonant frequency, influences  $v_g$ , since tank impedance is essentially zero

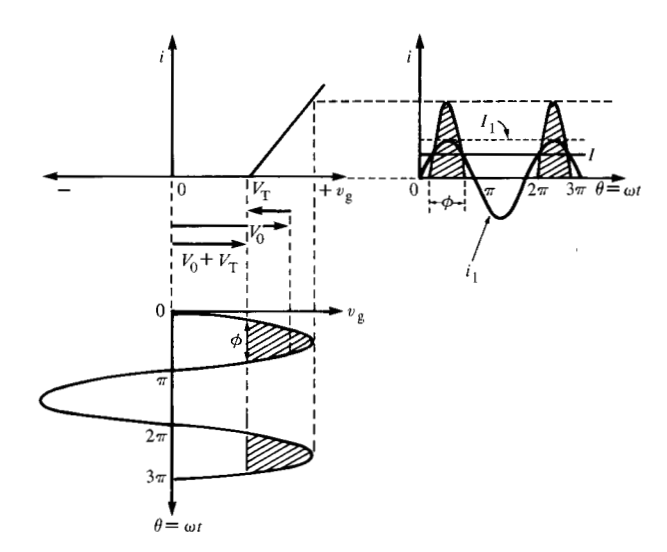


Figure A2 The oscillator-detector I-V relationships. The slope of the i- $v_{\rm g}$  transfer line shown is equal to  $g_{\rm m}[1/(1+g_{\rm m}R)]$ ,  $\phi$  is the conduction angle,  $i_1=I_1\sin\omega t$ , and  $v_{\rm g}=V_{\rm g}\sin\omega t$ . Note that the threshold voltage  $V_{\rm T}$  is negative.

at all higher harmonics. Thus,  $I_1 = I\{[2\cos{(\phi/2)}]/[1-(\phi/\pi)^2]\}$ , where I is the steady current delivered by the constant-dc-current generator. If we let  $[2\cos{(\phi/2)}]/[1-(\phi/\pi^2]=2\Psi$ , then  $V_{\rm g}=(\Psi Q I/2)(L/C)^{1/2}$  and for operating ranges over which there is very little change in  $\Psi$ , one observes that

$$V_g \approx k_2 Q.$$
 (A2)

## Oscillator-detector circuit analysis

In making decay-time measurements the linearly amplified output voltage  $V_0$  of Fig. A2 is observed. As we note from Eqs. (A1) and (A2), the observed signal will closely represent changes in wafer conductivity, provided the circuit response is

$$V_0 \approx k_3 V_g. \tag{A3}$$

This is confirmed both analytically and experimentally. For design optimization, one also needs quantitative relationships among  $V_0$ , tank Q, constant dc current source I, resistor R, and the ideal JFET parameters  $V_{\rm T}$  and  $g_{\rm m}$ . These relationships are determined by solution of a pair of simultaneous transcendental equations derived as follows. In Fig. A2, gate current will begin when  $v_{\rm gs}=0$ , at which point  $i=-g_{\rm m}V_{\rm T}$ ; for the conductivity range below this value  $i=g_{\rm m}(v_{\rm gs}-V_{\rm T})$  and i=0 whenever  $(v_{\rm gs}-V_{\rm T})$  is negative. For the operating region with drain potential always higher than the source potential and  $v_{\rm gs}<|0$ ,

$$v_{g} = V_{0} + iR + v_{gs}. \tag{A4}$$

Thus one obtains

$$i = [v_{\rm g} - (V_0 + V_{\rm T})] \frac{g_{\rm m}}{1 + g_{\rm R}}.$$
 (A5)

Figure A2 also shows the relationships involved in this equation, while graphically identifying the conduction angle  $\phi$  and the fundamental component  $i_1$  of drain current i.

Since no net charge is "lost" in C during each cycle, the transistor current pulses i flowing during conduction angle  $\phi$  carry the same charge as the constant current I flowing during  $\theta = 2\pi$  radians; i.e.,

$$I = \frac{1}{2\pi} \int_0^{2\pi} i \ d\theta = \frac{1}{2\pi} \int_{\frac{\pi}{2} - \frac{\phi}{2}}^{\frac{\pi}{2} + \frac{\phi}{2}} i \ d\theta. \tag{A6}$$

Substituting (A5) into (A6) and using  $v_{\rm g}=(\Psi QI/2)\times (L/C)^{1/2}\sin\omega t$ , one obtains

$$V_{0} = \frac{\Psi Q I (L/C)^{1/2} \sin (\phi/2)}{\phi} - V_{t} - \frac{2\pi I}{\phi} \left(\frac{1}{g_{m}} + R\right). \text{ (A7)}$$

This transcendental equation is one of two that must be solved simultaneously to determine oscillator  $\phi$  and the resulting detector output  $V_0$ , where other parameters are fixed. The second equation also derives from (A4). The onset of transistor conduction each cycle, with i arbitrarily close to zero, occurs at  $\omega t = (\pi/2) - (\phi/2)$ ; substituting this value and the term for  $v_{\rm g}$  just given into (A4) gives

$$V_0 = \frac{\Psi QI}{2} \left(\frac{L}{C}\right)^{1/2} \cos \frac{\phi}{2} - V_t.$$
 (A8)

Simultaneous solution of (A7) and (A8) for any desired values of  $g_{\rm m}$ ,  $V_{\rm T}$ ,  $\Psi Q$ , I, R, L, and C allows analysis (or optimization) of design. To accomplish this, a computer program was prepared that, for an entered set of desired circuit values, solved these equations separately for a succession of values of  $\phi$  and compared the resulting  $V_0$  values obtained. This was continued until the  $(\phi, V_0)$  pair providing the simultaneous solution was found.

An example of computed solutions is given in Fig. A3(a), for which the parameter values of one of our 150-MHz test instruments were entered into the program. Results of the three sets of calculations are shown, each set being solved for  $\Psi Q$  products of 40, 80, 120, 160, 176, and 200. The linearity of the experimental data points is essentially indistinguishable from these computed data for I=2 and 3 mA. For  $I \le 1$  mA, the actual transistor  $g_m$  has begun to drop below the ideal assumed value, giving expected lower sensitivity. Normal operation is at I=3 mA.

## • Practical circuit configuration

Figure A1(b) shows the schematic diagram of the final instrument. Component values are shown for the oscillator-detector portion; the remainder is a conventional circuit

low-noise broad-band preamplifier with maximum gain = 100 to drive the oscilloscope. The preamplifier input transistors are a matched JFET pair (dual 2N5163). This discrete component design was chosen since all integrated circuit operational amplifiers that we tried produced significantly higher output noise levels. When operating with detector output  $V_0 \approx 10 \text{ V}$ , the oscilloscope baseline indicates  $\approx 1-2$  mV of noise with preamplifier gain = 100. Thus, the detector output noise is of the order of only 10-20 μV. Typical photoinduced wafer conductivity changes produce signals of <0.5 mV at  $V_0$ . Even if Fig. A3(a) showed significant nonlinearity, this small fractional change in  $V_0$ , and thus in Q, would provide an almost ideal instrument transfer function. More detailed information on design considerations and operating constraints for this instrument is given in Ref. [2].

## • Practical instrument response

Considering Eqs. (A1)-(A3), one expects that the observed output voltage of the instrument should be a linear function of the conductivity of wafers coupled to the input. The preceding analysis indicates why this expectation is reasonable. Figure A3(b) is a plot of experimental data confirming the overall system linearity. As an indication of instrument sensitivity, note that the oscilloscope gain is normally set to display any  $500-\mu V$  portion of the vertical axis.

#### References

- 1. G. L. Miller, D. A. H. Robinson, and S. D. Ferris, Proceedings of the Topical Conference on Characterization of Semiconductor Materials and Devices: Semiconductor Characterization Techniques, P. A. Barnes and G. A. Rozgonyi, Eds. (Electronics Division Proceedings, Vol. 78-3), Electrochemical Society, Inc., Princeton, NJ, 1978, p. 1.
- H. W. Curtis and R. L. Verkuil, "A High Signal-to-Noise Oscillator for Contactless Measurement of Photoinduced Carrier Lifetimes," presented at the ASTM Symposium on Lifetime in Silicon, February 1979, San Diego, CA. (Proceedings to be published in book form.)
- S. M. Sze, Physics of Semiconductor Devices, John Wiley & Sons, Inc., New York, 1969, pp. 84-90.
- 4. Ibid, pp. 102-104.
- J. L. Moll, Physics of Semiconductors, McGraw-Hill Publishing Co., Inc., New York, 1964, p. 118.

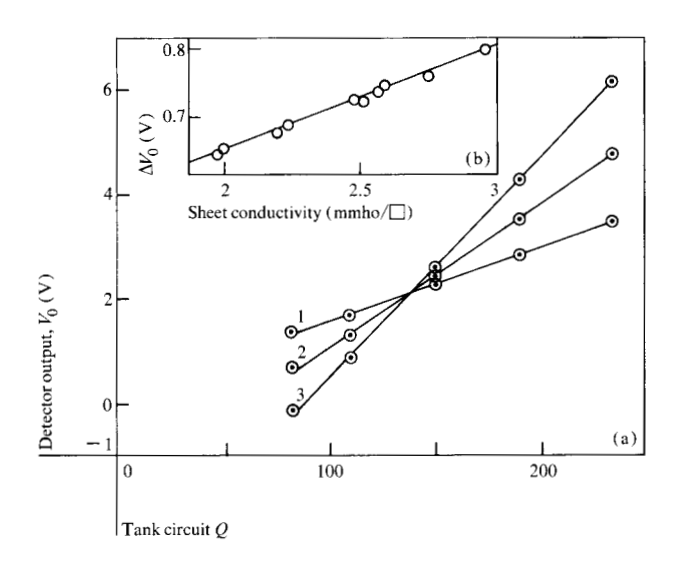


Figure A3 (a) Detector output as a function of tank circuit Q. Straight lines 1, 2, and 3 are fitted to data points for constant-decurrent generator I=1, 2, and 3 mA. The circled values are calculated by the simultaneous solutions described in the text. (b) Oscillator sensitivity to single wafer loading. The  $\Delta V_0$  equals the change in the digital voltmeter (DVM) reading when a wafer is placed on or removed from the instrument, where the coilwafer spacing = 3 mm; the data points indicate single wafer  $\Delta V_0$  values.

C. T. Sah, R. N. Noyce, and W. Shockley, "Carrier Generation and Recombination in p-n Junctions and p-n Junction Characteristics," *Proc. IRE*, 1234 (1957).

Received August 15, 1979; revised December 10, 1979

Roger Verkuil and Mun S. Pak are located at the IBM Data Systems Division laboratory, East Fishkill (Hopewell Junction), New York 12533. Huntington W. Curtis is with the IBM Information Records Division. His mailing address is IBM Biomedical Systems, 110 South Bedford Road, Mount Kisco, New York 10549.